

Article

# The Roles of Graphene and Ag in the Hybrid Ag@Ag<sub>2</sub>O-Graphene for Sulfamethoxazole Degradation

Li Zhou <sup>1,2</sup>, Guoyan Zou <sup>1,2,\*</sup> and Huiping Deng <sup>3,\*</sup>

<sup>1</sup> Institute of Eco-environment and Plant Protection, Shanghai Academy of Agricultural Sciences, Shanghai 201403, China; zhouli@saas.sh.cn

<sup>2</sup> Shanghai Engineering Research Centre of Low-Carbon Agriculture (SERCLA), Shanghai 201415, China

<sup>3</sup> College of Environmental State Key Laboratory of Pollution Control and Resource Reuse (Tongji University), Shanghai 200092, China

\* Correspondence: zouguoyan@263.net (G.Z.); denghuiping@tongji.edu.cn (H.D.); Tel.: +86-021-6220-2614 (G.Z.); +86-021-6220-2448 (H.D.)

Received: 24 May 2018; Accepted: 2 July 2018; Published: 4 July 2018



**Abstract:** Ag@Ag<sub>2</sub>O-graphene (Ag@Ag<sub>2</sub>O-G) with different concentrations of graphene was synthesized using a facile in situ precipitation method. The photocatalysts were characterized by field emission scanning electron microscopy (SEM), transmission electron microscopy (TEM), X-ray diffraction (XRD), and X-ray photoelectron spectroscopy (XPS), UV-vis diffuse reflectance spectra (DRS). The antibioticsulfamethoxazole (SMX) degradationunder simulated solar light and visible light irradiationwas investigated to evaluate photocatalytic performance. The composite photocatalyst Ag@Ag<sub>2</sub>O-G with 2.5 wt% graphene presented the highest activity among all the prepared composite photocatalysts. The coupling of graphene and Ag<sup>0</sup> increased the photocatalyticactivity and stability of pure Ag<sub>2</sub>O. Under higher SMX concentrations, the adsorption, not the photocatalytic ability, playeda crucial role during the SMX removal process. On the basis of the characterization and reactive oxygen species (ROS) scavenging experiments, a separation and transfer mechanism of photogenerated carriers was proposed. In the photocatalytic degradation of SMX, the major active species wereidentified as photogenerated holes; photogenerated electrons in the conduction band (CB) of Ag<sub>2</sub>O could not transfer to graphene through Ag<sup>0</sup>due to the more negative reduction potential of graphene. This is an important result regardinggraphene and Ag<sup>0</sup> roles which isdifferent from that for the photocatalytic degradation of dyes. This researchmay provide new insights into photocatalytic processes for the degradation of non-dye pollutants bycomposite materials to guidethe design of highly efficient reaction systems.

**Keywords:** Ag@Ag<sub>2</sub>O-graphene; graphene; Ag; visible light; sulfamethoxazole; photocatalytic mechanism

## 1. Introduction

Semiconductor photocatalysis, one of the most promising technologies for solar energy utilization and environmental remediation, has attracted tremendous attention since the semiconductor TiO<sub>2</sub> was applied to the decomposition of organic contaminants [1,2]. One of the most important objectives in semiconductor photocatalysis research is the development of efficient photocatalysts that can harvest visible light under sunlight. Although TiO<sub>2</sub>-based photocatalysts have been demonstrated to be efficient photocatalytic materials under visible light irradiation [3], the variety of visible light photocatalysts is still very limited, and the exploration of new and efficient photocatalytic materials sensitive to visible light remains challenging. Presently, some Ag-based semiconductors, such as Ag<sub>3</sub>PO<sub>4</sub> [4], AgCl [5], and Ag<sub>2</sub>O have gained attention because of their characteristics of easy visible light excitation and low mammalian toxicity. Among them, Ag<sub>2</sub>O, a brown powder with a simple cubic

structure and a lattice distance of 0.472 nm, has a narrow band-gap energy that can be easily excited by incident visible light [6]. However, after absorbing incident light, photons in  $\text{Ag}_2\text{O}$ , the photogenerated electrons in the conduction band (CB) are captured by surface lattice  $\text{Ag}^+$  ions to form  $\text{Ag}^0$  clusters, whereas photogenerated holes in the valence band (VB) oxidize lattice  $\text{O}^{2-}$  to release  $\text{O}_2$ , which results in the photodecomposition of  $\text{Ag}_2\text{O}$  and the formation of  $\text{Ag}^0$ . Therefore, pure  $\text{Ag}_2\text{O}$  has been rarely used as a visible light-driven photocatalyst because of its high photosensitivity and low-stability properties under light irradiation. There have been a few attempts to use  $\text{Ag}_2\text{O}$ -based materials as a photocatalyst under visible light irradiation.  $\text{Ag@Ag}_2\text{O}$ ,  $\text{AgBr/Ag}_2\text{O}$ ,  $\text{Ag}_2\text{O/TiO}_2$  heterostructure were introduced to decompose methyl orange (MO), and such attempts have exhibited high efficiency and stability [7–9]. These results indicate that  $\text{Ag}_2\text{O}$ -based materials have greater potential as stable and highly efficient photocatalysts than pure  $\text{Ag}_2\text{O}$  for photocatalytic decomposition of organic contaminants under visible light irradiation.

It is worthwhile to note that once a certain amount of  $\text{Ag}^0$  forms on the surface of  $\text{Ag}_2\text{O}$ , the following photogenerated electrons tend to transfer to the  $\text{Ag}^0$  sites and are captured by  $\text{O}_2$  [10]. To inhibit  $\text{Ag}_2\text{O}$  corrosion, it is expected that the photogenerated holes could transfer to other electron donors (such as organic substances), and the photogenerated electrons could transfer to other electron captures (such as  $\text{O}_2$ ) before reacting with lattice elements. It is possible that the produced  $\text{Ag}^0$  works as an electron pool and transfers the photogenerated electrons to improve photocatalytic activities. Therefore, the produced  $\text{Ag}^0$  could bring about an effective segregation capability of photo-excited electron-hole pairs and suppress  $\text{Ag}_2\text{O}$  photo-reduction. In order to address  $\text{Ag}_2\text{O}$  photocatalyst instability, a strategy of implementing hybrid material has been undertaken to determine an effective method to improve the catalytic activity and stability. Graphene, owing to its large specific area, flexible structure, high thermal and electrical conductivity, high chemical stability, and excellent electron capture and transport properties [11], could provide a supporting matrix to suppress the aggregation of nanoparticles and promote the effective separation of photogenerated carriers as an electron mediator for shuttling electrons [12]. Recently, combining graphene (G) with photocatalysts to enhance their photocatalytic performance has attracted considerable attention [13,14]. For example, the coupling of graphene with  $\text{TiO}_2$  could extend the light absorption from UV wavelengths into the visible region [15] and improve adsorption abilities and photocatalytic activities [16]. Graphene has been one of the most promising materials to enhance the photocatalytic performance in the new generation of photocatalysts [17]. However, in previous reports about  $\text{Ag@Ag}_3\text{PO}_4\text{-G}$  composite materials, the coupling graphene and  $\text{Ag}^0$  could not enhance its photocatalytic activity in organic pollutants degradation [4]. Therefore, the effects of graphene and  $\text{Ag}^0$  in composite photocatalysts remain unclear and deserve further research.

It should be noted that most previous studies of  $\text{Ag}_2\text{O}$ -based composite photocatalysts have focused on the decomposition of dyes, such as methyl orange (MO) [7], rhodamine B (RhB) [14], or methylene blue (MB) [18]. However, dyes used as photosensitization compounds could be excited by some wavelength lights to release electrons affecting the transfer of photogenerated carriers [19]. Other appropriate target pollutants should also be explored. The trace-level water contaminant sulfamethoxazole (SMX) can only absorb light at wavelengths lower than 320 nm [20], which makes SMX an ideal candidate to analyze photocatalytic activities and mechanisms of visible light-driven photocatalysts.

Herein, hybrid  $\text{Ag@Ag}_2\text{O-G}$  photocatalysts with different graphene concentrations were synthesized through a precipitation method. Photocatalytic activity of  $\text{Ag@Ag}_2\text{O-G}$  was evaluated by monitoring the degradation of SMX under simulated solar light ( $\lambda > 280$  nm) and visible light irradiation ( $\lambda > 400$  nm). In addition to photodegradation and adsorption abilities of  $\text{Ag@Ag}_2\text{O-G}$  on SMX, the stability of one of the photocatalysts after several recycles was also investigated. A possible photocatalytic degradation mechanism was proposed through investigation of the influence of reactive oxygen species (ROS) scavengers on  $\text{Ag@Ag}_2\text{O-G}$  photocatalytic activities. Through this research, the roles of graphene and  $\text{Ag}^0$  in the composite  $\text{Ag}_2\text{O}$ -based materials were investigated systemically

using SMX (non-photosensitizer, as target pollutant). This will provide new insights into photocatalytic mechanism analysis for composite photocatalysts.

## 2. Results and Discussions

### 2.1. Catalyst Characterization

Morphology of the as-prepared Ag@Ag<sub>2</sub>O-G2 was elucidated by SEM (scanning electron microscopy) and TEM (transmission electron microscopy), as shown in Figure 1a,b. It can be clearly seen that the Ag<sub>2</sub>O nanoparticles were close to spherical in shape with an average diameter of approximately 100 nm and covered by graphene with a folder surface. From the different colors of Figure 1b, the Ag<sub>2</sub>O particles in the dark color and graphene in the light color are clearly identified. The production of Ag on the surface of Ag<sub>2</sub>O particles was confirmed by the following XRD (X-ray diffraction) and XPS analysis.

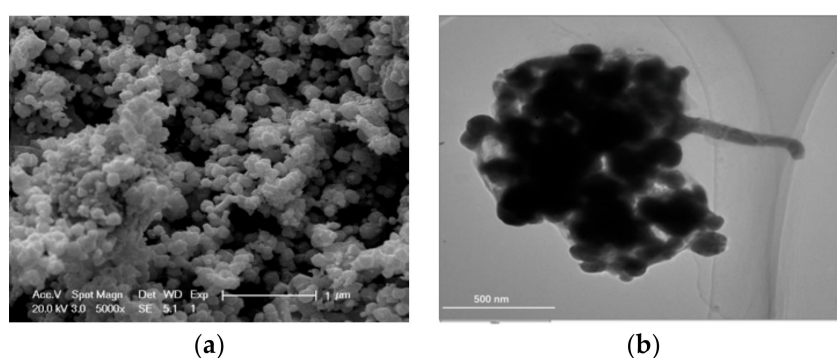


**Figure 1.** (a) SEM and (b) TEM images of Ag@Ag<sub>2</sub>O-G2 (with 2.5 wt% graphene).

XRD patterns of the pure Ag<sub>2</sub>O, Ag@Ag<sub>2</sub>O-G1, Ag@Ag<sub>2</sub>O-G2, and Ag@Ag<sub>2</sub>O-G3 are shown in Figure 2a. The diffraction peaks at  $2\theta = 32.8^\circ$ ,  $38.1^\circ$ ,  $54.9^\circ$ ,  $65.4^\circ$ , and  $68.8^\circ$  can be attributed to the respective (111), (200), (220), (311), and (222) planes of the cubic Ag<sub>2</sub>O (JCPDS No. 41-1104). No characteristic peak of graphene was observed in the patterns of composites, which might be ascribed to the high graphene dispersion. Compared with the pure Ag<sub>2</sub>O, the diffraction peaks of composite Ag@Ag<sub>2</sub>O-G2 at  $2\theta = 44.3^\circ$ ,  $64.4^\circ$  and  $77.5^\circ$  can be attributed to the cubic Ag (JCPDS No. 04-0783), which confirmed the formation of Ag. As shown in Figure 2b, the XPS peaks of Ag 3d also confirm the formation of Ag. The peaks centered at 368, and 374 eV corresponded to Ag 3d<sub>5/2</sub> and Ag 3d<sub>3/2</sub>, respectively. The Ag 3d<sub>5/2</sub> peak is divided into two different peaks at 368.6 and 368.1 eV, and the Ag 3d<sub>3/2</sub> peak is divided into 374.6 and 374.1 eV, respectively. The peaks at 368.6 and 374.6 eV are attributed to Ag, whereas the peaks at 368.1 and 374.1 eV are attributed to Ag<sup>+</sup> in Ag<sub>2</sub>O, and the two pairs of separated silver peaks show a difference of  $D = 6$  eV [21]. The molar content of the surface metallic Ag is calculated to be 11.2 wt% of the total silver element in Ag@Ag<sub>2</sub>O-G2 according to the areas of divided peaks (as shown in Figure 2b). The XPS peak corresponded highly to the XRD analysis, proving the co-existence of Ag and Ag<sub>2</sub>O in the composite.

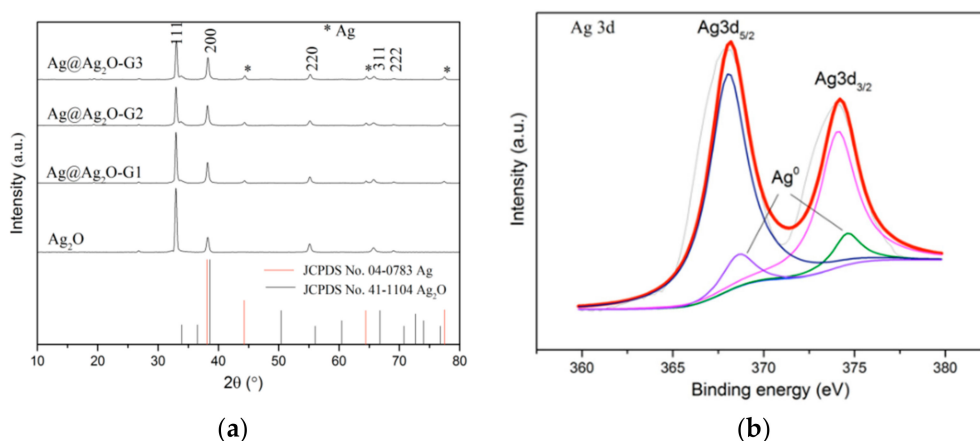


**Figure 2.** (a) XRD patterns of  $\text{Ag}_2\text{O}$ ,  $\text{Ag@Ag}_2\text{O-G1}$ ,  $\text{Ag@Ag}_2\text{O-G2}$ ,  $\text{Ag@Ag}_2\text{O-G3}$  and XPS peaks of (b) Ag 3d in  $\text{Ag@Ag}_2\text{O-G2}$ .

## 2.2. Photocatalytic Performance

As shown in Figure 3a–c, after adsorption in the dark for 30 min, the adsorption capacity of  $\text{Ag}_2\text{O}$ ,  $\text{Ag@Ag}_2\text{O-G1}$ ,  $\text{Ag@Ag}_2\text{O-G2}$ , and  $\text{Ag@Ag}_2\text{O-G3}$  were 2.77, 4.77, 5.17, and 5.48 mg/g respectively. The addition of graphene in  $\text{Ag@Ag}_2\text{O-G1}$ ,  $\text{Ag@Ag}_2\text{O-G2}$ , and  $\text{Ag@Ag}_2\text{O-G3}$  increased 72.2%, 86.6%, and 97.8% of adsorption capacity than pure  $\text{Ag}_2\text{O}$ , respectively. Under a different light source,  $\text{Ag}_2\text{O}$ -based photocatalysts showed the same trend in SMX degradation. The SMX concentration in the solution increased rapidly after irradiation, thus indicating that desorption had occurred. For  $\text{Ag}_2\text{O}$ ,  $\text{Ag@Ag}_2\text{O-G1}$ ,  $\text{Ag@Ag}_2\text{O-G2}$ , and  $\text{Ag@Ag}_2\text{O-G3}$ , the desorption percentages were 71.59%, 43.69%, 37.30%, and 35.94% under simulated solar light and 69.83%, 40.81%, 36.48%, and 33.85% under visible light, respectively. It was concluded that the light of the UV part of the simulated solar light could result in more  $\text{Ag}_2\text{O}$  corrosion, which desorbs the SMX more than visible light [9]. The relationship between  $\ln(C_5/C_{T-5})$  ( $C_5$ , the initial concentration of SMX after 5 min irradiation and  $C_{T-5}$ , the concentration of SMX after (T-5) min irradiation) and irradiation time followed first-order kinetics. The basic kinetic parameters for the  $\text{Ag}_2\text{O}$  series photocatalysts under different light irradiations are shown in Table S1. Obtained values of the apparent rate constants were 0.016, 0.0353, 0.045, and 0.027  $\text{min}^{-1}$  under simulated solar light and 0.012, 0.0340, 0.038, and 0.028  $\text{min}^{-1}$  under visible light ( $R^2 > 0.96$ ). The difference between photocatalytic activities under simulated solar light and visible light was not significant because of the similar light intensity (37.7  $\text{mW}/\text{cm}^2$  for simulated solar light and 34.2  $\text{mW}/\text{cm}^2$  for visible light). The adsorption capacity increased and the desorption percentages decreased with the additional graphene and the  $\text{Ag}^0$  produced in the photocatalysts. However, the photocatalytic activities were not in linear relation with the graphene addition, and the  $\text{Ag@Ag}_2\text{O-G2}$  with 2.5 wt% of graphene content showed the highest degradation efficiency for SMX removal. The photocatalytic performance deteriorated when the graphene dosage was increased above its optimal value. This phenomenon could be because graphene absorbs some light and, thus, might cause a light harvesting competition between  $\text{Ag}_2\text{O}$  and graphene with the increasing graphene concentration [22], which was consistent with light absorption abilities of photocatalysts (as shown in Figure S1). On the other hand, the photogenerated  $\text{Ag}^0$  on the surface of  $\text{Ag}_2\text{O}$  enhanced its structural stability due to a self-stability mechanism [10] that decreased the photocatalyst corrosion and SMX desorption percentages. In order to avoid photocatalyst corrosion, visible light was adopted to conduct further experiments.

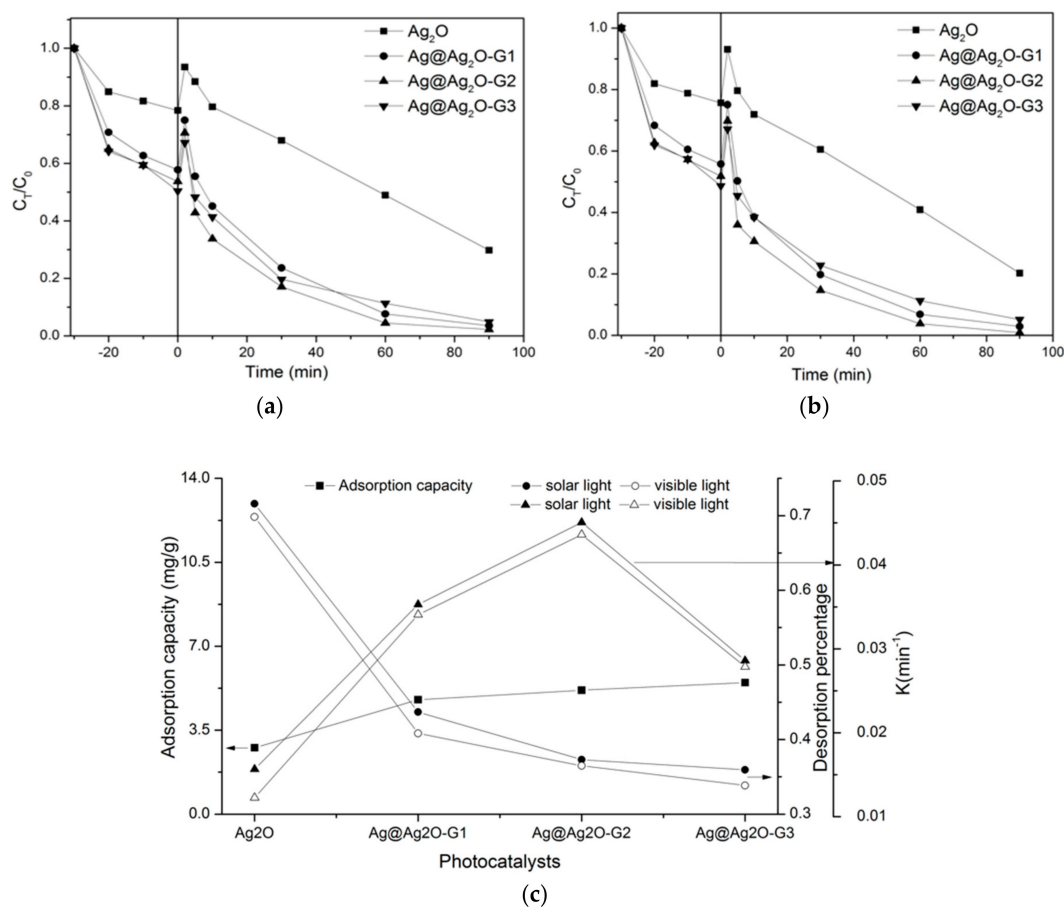


**Figure 3.** Adsorption abilities and photocatalytic activities of  $Ag_2O$ ,  $Ag@Ag_2O-G1$ ,  $Ag@Ag_2O-G2$ ,  $Ag@Ag_2O-G3$  for SMX removal under (a) simulated solar light ( $\lambda > 280$  nm), (b) visible light ( $\lambda > 400$  nm) irradiation ( $C_{SMX} = 1$  mg/L,  $C_{catalysts} = 0.05$  g/L), and (c) the adsorption capacity of photocatalysts and a comparison of the desorption percentage and pseudo-first-order reaction rate under different light irradiation.

The results of adsorption and photocatalytic degradation in different SMX concentrations are shown in Figure 4. In the higher concentrations of 2.5, 5, and 10 mg/L, the SMX was mostly removed by adsorption. The adsorption capacities of  $Ag@Ag_2O-G2$  for 1, 2.5, 5, and 10 mg/L SMX were 5.0, 23.6, 47.4, and 98.4 mg/L, respectively (as shown in Figure 4a). As the SMX concentrations were increased, the adsorption capacity of the photocatalyst also obviously increased, and almost no degradation products were detected after 10 mg/L SMX was adsorbed and photocatalytically degraded (as shown in Figure 5b). However, with the exception of an SMX substance peak at 4.11 min for 1 mg/L SMX, there were some other peaks for degradation products identified by high-performance liquid chromatography (HPLC) (as shown in Figure 5a). The results indicate that the photocatalyst adsorption ability was not positively related to the photocatalytic activity, which is consistent with the results of previous research [23]. This may be ascribed to the competition of light absorption between the photocatalyst and pollutants. The higher SMX concentration beyond the value of 2.5 mg/L with multilayer SMX coverage on the photocatalyst weakens the radiant flux necessary for the  $Ag_2O$  [24], which explains the phenomenon that no obvious desorption occurred after 5 min irradiation under a higher SMX concentration ( $\geq 2.5$  mg/L).

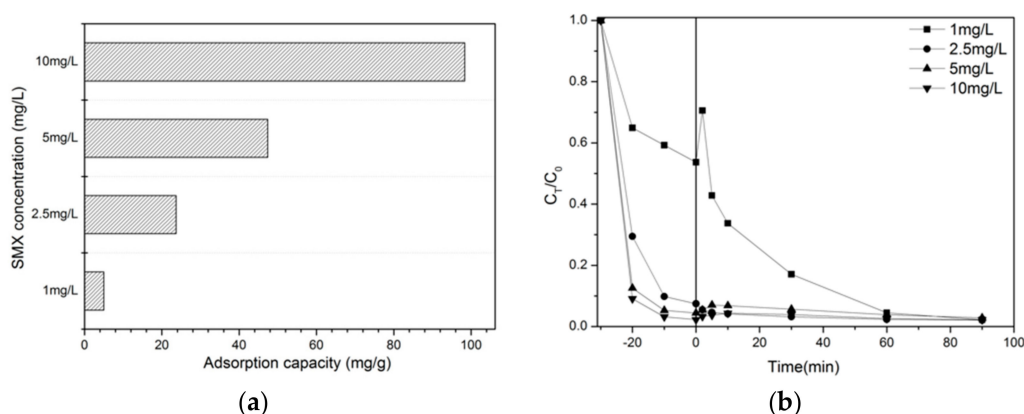


**Figure 4.** (a) Adsorption capacity of Ag@Ag<sub>2</sub>O-G2 for different SMX concentrations in the dark and (b) adsorption capacity and the photocatalytic activities of Ag@Ag<sub>2</sub>O-G2 for different SMX concentrations removal under visible light (C<sub>catalyst</sub> = 0.05 g/L).

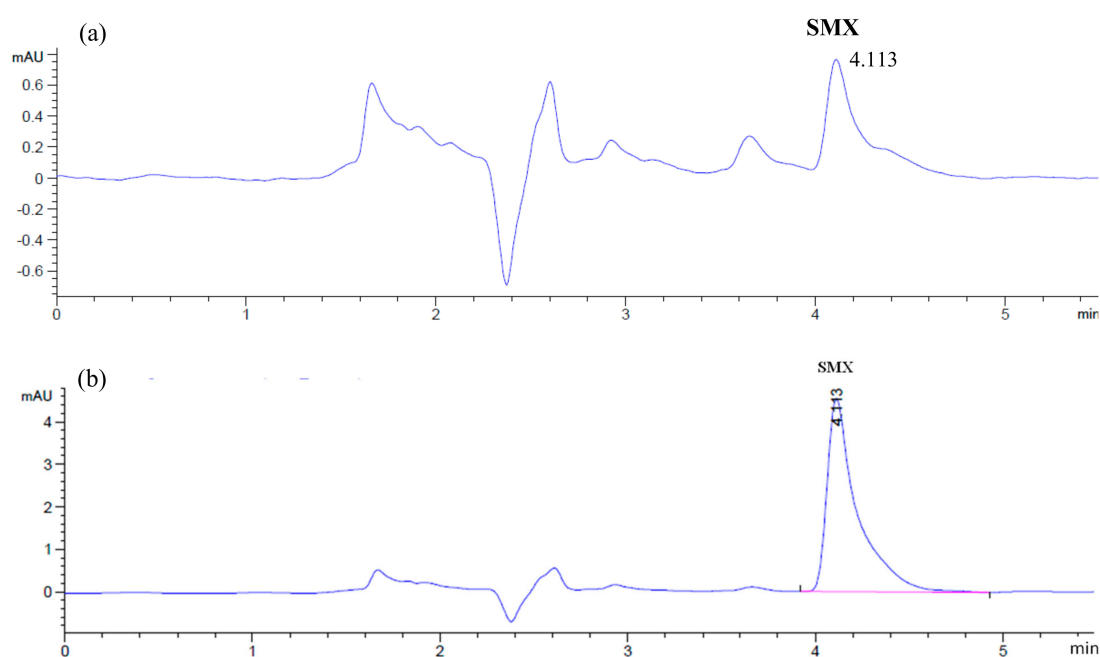


**Figure 5.** HPLC tests of (a) 1 mg/L, and (b) 10 mg/L SMX after adsorption and degradation by Ag@Ag<sub>2</sub>O-G2 under visible light.

### 2.3. Photocatalyst Stability

As shown in Figure 6, in the first two successive experimental runs (a total of four hours), SMX removal by adsorption and photocatalytic degradation of Ag@Ag<sub>2</sub>O-G2 remained almost the same. However, the SMX removal percentage decreased from almost 100% to approximately 40% in the third run and almost all of it was removed by adsorption. When the SMX concentration was 2.5 mg/L, the adsorption ability was crucial to the removal of SMX. After the photocatalyst was recycled twice, the SMX removal efficiency decreased rapidly in the third recycle due to adsorption capacity saturation and more photocorrosion occurred in the photocatalyst (as shown in Figure S2). It could be concluded that the Ag@Ag<sub>2</sub>O-G2 has the ability to photocatalytically oxidize low-concentration SMX ( $\leq 1$  mg/L) and adsorb high-concentration SMX ( $\geq 2.5$  mg/L).

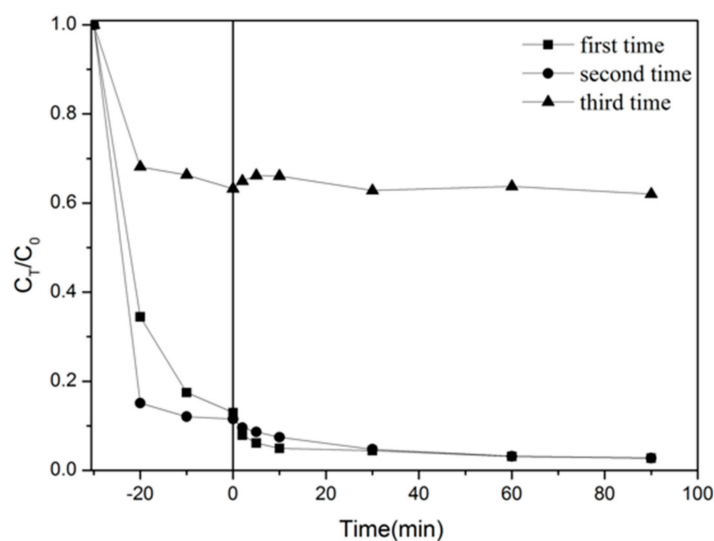


**Figure 6.** Repeated adsorption and photocatalytic degradation of SMX under visible light by Ag@Ag<sub>2</sub>O-G2 ( $C_{\text{catalyst}} = 0.25$  g/L,  $C_{\text{SMX}} = 2.5$  mg/L).

#### 2.4. Mechanism Analysis

In the photocatalytic system ( $C_{\text{SMX}} = 1$  mg/L,  $C_{\text{Ag@Ag}_2\text{O-G2}} = 0.05$  g/L), the oxidative species were probed by scavenger addition into the solution. The results in Figure 7 show that benzoquinone and sodium azide addition had negligible effects, while isopropanol addition had a slight effect on SMX photodegradation. The results indicated that the main reactive oxygen species were not  $\bullet\text{OH}$ ,  $\text{O}_2\bullet^-$  and  $^1\text{O}_2$  in this photocatalytic process. A rapid termination of photocatalysis was investigated after Na<sub>2</sub>-EDTA addition and only 5.2% of SMX was removed after 90 min of irradiation. One possible explanation is that, on the surface of the photocatalyst, the deposited EDTA anion as a hole trap blocked the reaction sites. This implies that the SMX oxidation process occurred on the surface of photocatalyst, and photogenerated holes were the main reactive species.

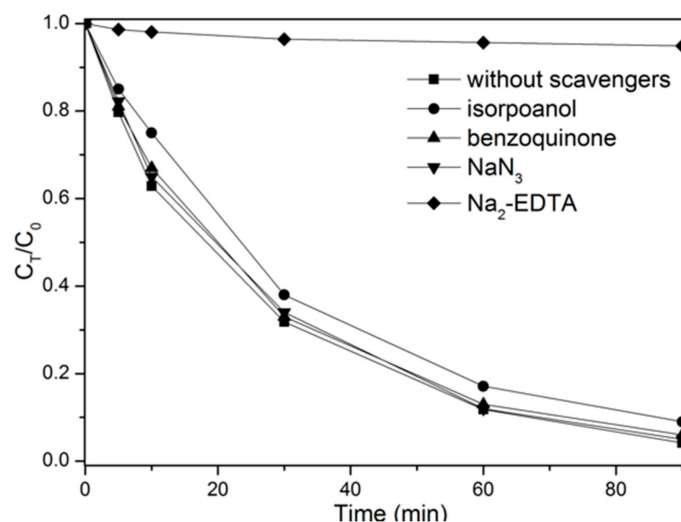


**Figure 7.** Photocatalytic activities of Ag@Ag<sub>2</sub>O-G2 in the reactive species scavenging experiments under visible light.

The schematics of the possible charge transfer and oxidation processes under visible light irradiation are illustrated in Figure 8. Ag<sub>2</sub>O was excited to photogenerated electrons and holes in its CB

and VB. The CB and VB potentials of  $\text{Ag}_2\text{O}$  were +0.20 and +1.50 V [25] (as shown in Figure 8) versus a normal hydrogen electrode (NHE), respectively. The holes in the VB of the  $\text{Ag}_2\text{O}$  (+1.50 V/NHE) could degrade the SMX (+0.9 V/NHE [26]) to  $\text{CO}_2$  or to other intermediates, but they could not oxidize the  $\text{OH}^-$  to  $\bullet\text{OH}$  (+1.89 V/NHE [27]) or  $\text{H}_2\text{O}$  to  $\bullet\text{OH}$  (+2.68 V/NHE [28]). The electrons in the CB of the  $\text{Ag}_2\text{O}$  (+0.20 V/NHE) could not reduce the  $\text{O}_2$  to  $\text{O}_2\bullet^-$  (-0.33 V/NHE) and  $\text{HO}_2\bullet$  (-0.55 V/NHE) [29]. However, the electrons could reduce the  $\text{O}_2$  to  $\text{H}_2\text{O}_2$  (+0.695 V/NHE) [29] through a two-electron reduction [30] and then continue to react with electrons to produce active  $\bullet\text{OH}$  [31], as verified by the scavenging experiments. The  $\text{Ag}^0$  produced in the catalyst preparation process could act as electron capture centers [32], and transfer electrons in the CB of the  $\text{Ag}_2\text{O}$  to oxygen through multi-electron-transfer routes. In other studies, graphene has been considered effective in reducing the combination rate of photogenerated electron-hole pairs when coupling with semiconductors owing to the electron shuttle from the conjugated carbon network [22]. However, the electrons in the CB of the  $\text{Ag}_2\text{O}$  could not transfer to the graphene through  $\text{Ag}^0$  because of the more negative graphene reduction potential (-0.11 V) [19,33], which indicated that graphene could increase photocatalytic activities only through higher adsorption capacity and more active sites to anchor the SMX. Therefore, in the  $\text{Ag@Ag}_2\text{O-G}$  photocatalytic system, the major active species for photocatalytic degradation were identified as the holes, while graphene was identified as the adsorbent and  $\text{Ag}^0$  as the electron capture center, which increased the  $\text{Ag}_2\text{O}$  photocatalytic activities to remove the SMX and the stability of photocatalysts.

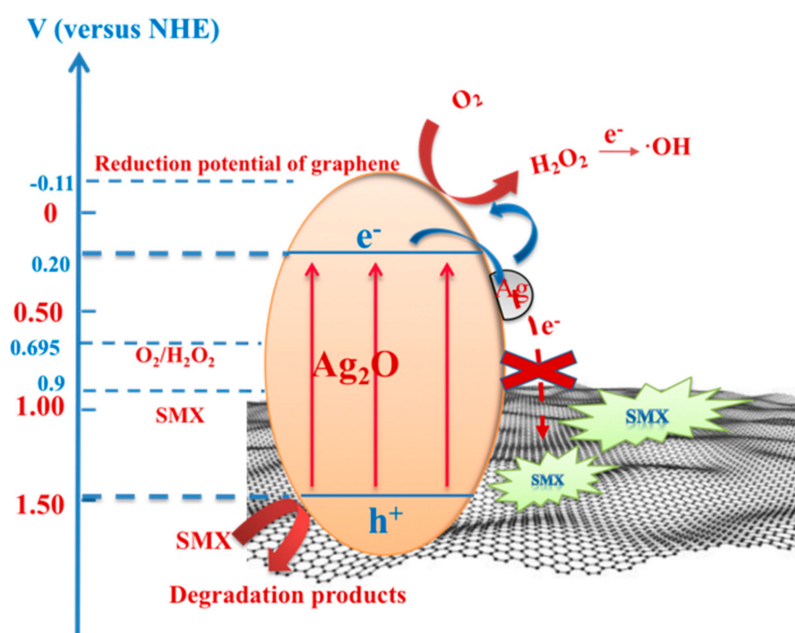


**Figure 8.** The charge separation and transfer in SMX photodegradation over the  $\text{Ag@Ag}_2\text{O-G}$  catalysts under visible light.

### 3. Materials and Methods

#### 3.1. Catalyst Preparation

Silver nitrate ( $\text{AgNO}_3$ ), sodium hydroxide ( $\text{NaOH}$ ), ammonia solution (25–28%), ethanol (>99.7%) were purchased from Sinopharm Chemical Reagent Co., Ltd. (Shanghai, China). Graphene was purchased from Nanjing XFNANO Materials Tech Co., Ltd. (Nanjing, China). All chemicals used in this study were of analytical grade without further purification. In a typical synthesis of the  $\text{Ag@Ag}_2\text{O-G}$  composite, solutions of 50 mL of 0.2 M  $\text{AgNO}_3$ , 100 mL of 0.2 M ammonia water, and 100 mL of 2 M  $\text{NaOH}$  were prepared in advance. The ammonia water was added to the

AgNO<sub>3</sub> solution slowly, changing the color of the solution from yellowish-brown to transparent—thus, creating a silver-ammonia solution. A certain amount of graphene powder was then dispersed into the silver-ammonia solution and sonicated for 2 h. Afterwards, the NaOH solution was dropped into the silver-ammonia solution with added graphene to form black Ag<sub>2</sub>O-G. To synthesize the Ag@Ag<sub>2</sub>O-G, the Ag<sub>2</sub>O-G suspension was irradiated for 3 h using a 300 W Xe lamp equipped with an optical cut-off filter ( $\lambda > 400$  nm). The resultant Ag@Ag<sub>2</sub>O-G was separated by centrifugation (1000 rpm for 30 min), and then washed with Milli-Q water and ethanol several times and freeze-dried under a vacuum. According to the graphene concentrations of 1.7, 2.5, and 3.4 wt%, the obtained samples were labeled as Ag@Ag<sub>2</sub>O-G1, Ag@Ag<sub>2</sub>O-G2, and Ag@Ag<sub>2</sub>O-G3. For comparison, the same procedure without graphene and irradiation was carried out to obtain pure Ag<sub>2</sub>O.

### 3.2. Catalyst Characterization

Sample morphology was examined by transmission electron microscopy (TEM) (CM200FEG, Philips, Amsterdam, The Netherlands) and scanning electron microscopy (SEM) (XL30FEG, Philips, The Netherlands). Analyses by X-ray diffraction (XRD) were performed with a Bruker D8 Advance diffractometer with Cu-K $\alpha$  radiation (Optik GmbH, Ettlingen, Germany). Experiments using an X-ray photoelectron spectroscopy (XPS) (PHI, Chanhassen, MN, USA) were carried out on an RBD (RBD Instruments, Bend, OR, USA) upgraded PHI-5000C ESCA system (Perkin Elmer, Waltham, MA, USA) with Mg-K $\alpha$  radiation ( $h = 1253.6$  eV). UV-vis diffuse reflectance spectra (DRS) were measured by a Shimadzu UV-2550 spectrometer (Shimadzu Corporation, Kyoto, Japan), while BaSO<sub>4</sub> was used as the reference.

### 3.3. Analysis Method

The SMX concentration was quantified by high-performance liquid chromatography (HPLC) supplied by Agilent with a Teknokroma C-18 Tracer Extrasil ODS2 (Teknokroma, Barcelona, Spain) (250 mm  $\times$  4.6 mm). The mobile phase was a mixture of 40% acetonitrile and 60% water which was adjusted at pH = 3 with phosphoric acid. The analysis was performed under isocratic conditions at a flow rate of 1 mL/min, with an injection volume of 10  $\mu$ L and an oven temperature of 25  $^{\circ}$ C. The wavelength of the UV detector was set at 270 nm.

### 3.4. Photocatalytic Degradation of SMX

The photocatalytic experiments for SMX removal were conducted with a 300 W xenon lamp with a cut-off filter ( $\lambda > 280$  nm) as a simulated solar light source and a cut-off filter ( $\lambda > 400$  nm) as the visible light source. The light intensity on the surface of the suspension was kept at 37.7 mW/cm<sup>2</sup> for simulated solar light and 34.2 mW/cm<sup>2</sup> for visible light. SMX photocatalytic oxidation was completed in a 250 mL beaker with a cooling system on the bottom to maintain a constant solution temperature of 25  $\pm$  2  $^{\circ}$ C. In a typical experiment, 5 mg of photocatalysts were suspended in 100 mL of 1 mg/L SMX solution by ultrasonication for 5 min. Before irradiation, the mixture suspension was stirred thoroughly in the dark for 30 min to ensure an adsorption-desorption equilibrium between the SMX and the photocatalyst. The lamp was then switched on to initiate the photocatalytic reaction. 3 mL of solution was sampled at certain time intervals and filtered with 0.45  $\mu$ m syringe filters to remove suspended photocatalysts for the SMX analysis. Experiments for different SMX concentrations were conducted ( $C_{\text{catalyst}} = 0.05$  g/L,  $C_{\text{SMX}} = 1, 2.5, 5, 10$  mg/L) using the same procedures. Investigation of the reactive oxidative species was similar to the photodegradation process, while the scavengers (10 mM of iso-propanol, 0.5  $\mu$ M of benzoquinone, 0.5  $\mu$ M of sodium azide (NaN<sub>3</sub>) and 5 mM of disodium ethylene diamine tetraacetate (Na<sub>2</sub>-EDTA)) were added to the SMX solution prior to addition of the photocatalyst. In the recycling experiments, higher concentrations of photocatalysts and SMX ( $C_{\text{catalyst}} = 0.25$  g/L,  $C_{\text{SMX}} = 5$  mg/L) were used. The used photocatalysts were separated from the solution and then washed with Milli-Q water thoroughly before being re-dispersed in the fresh SMX solution for another cycle.

#### 4. Conclusions

A hybrid Ag@Ag<sub>2</sub>O-graphene photocatalyst was synthesized with a facile chemical precipitation approach and reduction procedure under visible light. The Ag@Ag<sub>2</sub>O-G2 with 2.5 wt% of graphene content possessed a higher activity than the other prepared composite photocatalysts with 1.7 and 3.4 wt% of graphene content. The addition of graphene and produced Ag<sup>0</sup> not only increased the photocatalyst adsorption capacities, but also decreased desorption percentages after irradiation. Under a higher SMX concentration, the adsorption, but not the photocatalytic ability, played a crucial role during the SMX removal process. The Ag@Ag<sub>2</sub>O-G2 showed stable photocatalytic activities in at least two successive experimental runs (a total of four hours). During the photocatalytic processes of Ag@Ag<sub>2</sub>O-G2, the generated holes were dominant reactive oxygen species for the photocatalytic degradation of SMX and Ag<sup>0</sup>, as the electron capture center could not transfer electrons in the CB of the Ag<sub>2</sub>O to graphene due to the negative graphene reduction potential.

**Supplementary Materials:** The following are available online at <http://www.mdpi.com/2073-4344/8/7/272/s1>, Figure S1: UV-vis spectra of Ag<sub>2</sub>O, Ag@Ag<sub>2</sub>O-G1, Ag@Ag<sub>2</sub>O-G2 and Ag@Ag<sub>2</sub>O-G3, Table S1: The rate constants and R<sup>2</sup> of first order kinetic reaction for Ag<sub>2</sub>O, Ag@Ag<sub>2</sub>O-G1, Ag@Ag<sub>2</sub>O-G2 and Ag@Ag<sub>2</sub>O-G3 to degrade SMX, Figure S2: XPS spectra of Ag 3d in Ag@Ag<sub>2</sub>O-G2 before and after recycle use.

**Author Contributions:** L.Z., G.Z. and H.D. conceived and designed the experiments; L.Z. performed the experiments; L.Z. and G.Z. analyzed the data; H.D. contributed reagents/materials/analysis tools; L.Z. wrote the paper.

**Acknowledgments:** This work was financially supported by the Chinese Ministry of Construction Foundation for Major Special projects of Water Pollution Control and Management of Science & Technology (No. 2017ZX07201-003 and No. 2017ZX07202004-004).

**Conflicts of Interest:** The authors declare no conflict of interest.

#### References

1. Ravelli, D.; Dondi, D.; Fagnoni, M.; Albini, A. Photocatalysis. A multi-faceted concept for green chemistry. *Chem. Soc. Rev.* **2009**, *38*, 1999–2011. [[CrossRef](#)] [[PubMed](#)]
2. Schneider, J.; Matsuoka, M.; Takeuchi, M.; Zhang, J.; Horiuchi, Y.; Anpo, M.; Bahnemann, D.W. Understanding TiO<sub>2</sub> Photocatalysis: Mechanisms and Materials. *Chem. Rev.* **2014**, *114*, 9919–9986. [[CrossRef](#)] [[PubMed](#)]
3. Dahl, M.; Liu, Y.; Yin, Y. Composite Titanium Dioxide Nanomaterials. *Chem. Rev.* **2014**, *114*, 9853–9889. [[CrossRef](#)] [[PubMed](#)]
4. Zhou, L.; Alvarez, O.G.; Mazon, C.S.; Chen, L.; Deng, H.; Sui, M. The roles of conjugations of graphene and Ag in Ag<sub>3</sub>PO<sub>4</sub>-based photocatalysts for degradation of sulfamethoxazole. *Catal. Sci. Technol.* **2016**, *6*, 5972–5981. [[CrossRef](#)]
5. Choi, M.; Shin, K.-H.; Jang, J. Plasmonic photocatalytic system using silver chloride/silver nanostructures under visible light. *J. Colloid Interface Sci.* **2010**, *341*, 83–87. [[CrossRef](#)] [[PubMed](#)]
6. Xu, H.; Xie, J.; Jia, W.; Wu, G.; Cao, Y. The formation of visible light-driven Ag/Ag<sub>2</sub>O photocatalyst with excellent property of photocatalytic activity and photocorrosion inhibition. *J. Colloid Interface Sci.* **2018**, *516*, 511–521. [[CrossRef](#)] [[PubMed](#)]
7. Jiang, W.; Wang, X.; Wu, Z.; Yue, X.; Yuan, S.; Lu, H.; Liang, B. Silver Oxide as Superb and Stable Photocatalyst under Visible and Near-Infrared Light Irradiation and Its Photocatalytic Mechanism. *Ind. Eng. Chem. Res.* **2015**, *54*, 832–841. [[CrossRef](#)]
8. Cao, Y.; Li, Q.; Xing, Y.; Zong, L.; Yang, J. In situ anion-exchange synthesis and photocatalytic activity of AgBr/Ag<sub>2</sub>O heterostructure. *Appl. Surf. Sci.* **2015**, *341*, 190–195. [[CrossRef](#)]
9. Zhou, W.; Liu, H.; Wang, J.; Liu, D.; Du, G.; Cui, J. Ag<sub>2</sub>O/TiO<sub>2</sub> Nanobelts Heterostructure with Enhanced Ultraviolet and Visible Photocatalytic Activity. *ACS Appl. Mater. Interfaces* **2010**, *2*, 2385–2392. [[CrossRef](#)] [[PubMed](#)]
10. Wang, X.; Li, S.; Yu, H.; Yu, J.; Liu, S. Ag<sub>2</sub>O as a New Visible-Light Photocatalyst: Self-Stability and High Photocatalytic Activity. *Chem. Eur. J.* **2011**, *17*, 7777–7780. [[CrossRef](#)] [[PubMed](#)]

11. Ma, D.; Wu, J.; Gao, M.; Xin, Y.; Ma, T.; Sun, Y. Fabrication of Z-scheme g-C<sub>3</sub>N<sub>4</sub>/RGO/Bi<sub>2</sub>WO<sub>6</sub> photocatalyst with enhanced visible-light photocatalytic activity. *Chem. Eng. J.* **2016**, *290*, 136–146. [[CrossRef](#)]
12. Shen, H.; Wang, J.; Jiang, J.; Luo, B.; Mao, B.; Shi, W. All-solid-state Z-scheme system of RGO-Cu<sub>2</sub>O/Bi<sub>2</sub>O<sub>3</sub> for tetracycline degradation under visible-light irradiation. *Chem. Eng. J.* **2017**, *313*, 508–517. [[CrossRef](#)]
13. Hu, X.; Liu, X.; Tian, J.; Li, Y.; Cui, H. Towards full-spectrum (UV, visible, and near-infrared) photocatalysis: Achieving an all-solid-state Z-scheme between Ag<sub>2</sub>O and TiO<sub>2</sub> using reduced graphene oxide as the electron mediator. *Catal. Sci. Technol.* **2017**, *7*, 4193–4205. [[CrossRef](#)]
14. Ran, R.; Meng, X.; Zhang, Z. Facile preparation of novel graphene oxide-modified Ag<sub>2</sub>O/Ag<sub>3</sub>VO<sub>4</sub>/AgVO<sub>3</sub> composites with high photocatalytic activities under visible light irradiation. *Appl. Catal. B-Environ.* **2016**, *196*, 1–15. [[CrossRef](#)]
15. Giovannetti, R.; Rommozzi, E.; Zannotti, M.; D'Amato, C.A. Recent Advances in Graphene Based TiO<sub>2</sub> Nanocomposites (GTiO<sub>2</sub>Ns) for Photocatalytic Degradation of Synthetic Dyes. *Catalysts* **2017**, *7*, 305. [[CrossRef](#)]
16. Giovannetti, R.; Rommozzi, E.; Zannotti, M.; D'Amato, C.A.; Ferraro, S.; Cespi, M.; Bonacucina, G.; Minicucci, M.; Di Cicco, A. Exfoliation of graphite into graphene in aqueous solution: An application as graphene/TiO<sub>2</sub> nanocomposite to improve visible light photocatalytic activity. *RSC Adv.* **2016**, *6*, 93048–93055. [[CrossRef](#)]
17. Truppi, A.; Petronella, F.; Placido, T.; Striccoli, M.; Agostiano, A.; Curri, M.L.; Comparelli, R. Visible-Light-Active TiO<sub>2</sub>-Based Hybrid Nanocatalysts for Environmental Applications. *Catalysts* **2017**, *7*, 100. [[CrossRef](#)]
18. Ji, Z.; Shen, X.; Yang, J.; Xu, Y.; Zhu, G.; Chen, K. Graphene Oxide Modified Ag<sub>2</sub>O Nanocomposites with Enhanced Photocatalytic Activity under Visible-Light Irradiation. *Eur. J. Inorg. Chem.* **2013**, *2013*, 6119–6125. [[CrossRef](#)]
19. Dong, P.; Wang, Y.; Cao, B.; Xin, S.; Guo, L.; Zhang, J.; Li, F. Ag<sub>3</sub>PO<sub>4</sub>/reduced graphite oxide sheets nanocomposites with highly enhanced visible light photocatalytic activity and stability. *Appl. Catal. B-Environ.* **2013**, *132–133*, 45–53. [[CrossRef](#)]
20. Moore, D.E.; Zhou, W. Photodegradation of sulfamethoxazole—a chemical-system capable of monitoring seasonal-changes in UVB intensity. *Photochem. Photobiol.* **1994**, *59*, 497–502. [[CrossRef](#)] [[PubMed](#)]
21. Yang, H.; Tian, J.; Li, T.; Cui, H. Synthesis of novel Ag/Ag<sub>2</sub>O heterostructures with solar full spectrum (UV, visible and near-infrared) light-driven photocatalytic activity and enhanced photoelectrochemical performance. *Catal. Commun.* **2016**, *87*, 82–85. [[CrossRef](#)]
22. Dong, S.; Ding, X.; Guo, T.; Yue, X.; Han, X.; Sun, J. Self-assembled hollow sphere shaped Bi<sub>2</sub>WO<sub>6</sub>/RGO composites for efficient sunlight-driven photocatalytic degradation of organic pollutants. *Chem. Eng. J.* **2017**, *316*, 778–789. [[CrossRef](#)]
23. Parra, S.; Olivero, J.; Pulgarin, C. Relationships between physicochemical properties and photoreactivity of four biorecalcitrant phenylurea herbicides in aqueous TiO<sub>2</sub> suspension. *Appl. Catal. B-Environ.* **2002**, *36*, 75–85. [[CrossRef](#)]
24. Bandara, J.; Mielczarski, J.A.; Kiwi, J. 2. Photosensitized degradation of azo dyes on Fe, Ti, and Al oxides. Mechanism of charge transfer during the degradation. *Langmuir* **1999**, *15*, 7680–7687. [[CrossRef](#)]
25. Shi, L.; Liang, L.; Ma, J.; Wang, F.; Sun, J. Enhanced photocatalytic activity over the Ag<sub>2</sub>O-g-C<sub>3</sub>N<sub>4</sub> composite under visible light. *Catal. Sci. Technol.* **2014**, *4*, 758–765. [[CrossRef](#)]
26. Gagné, F.; Blaise, C.; André, C. Occurrence of pharmaceutical products in a municipal effluent and toxicity to rainbow trout (*Oncorhynchus mykiss*) hepatocytes. *Ecotoxicol. Environ. Saf.* **2006**, *64*, 329–336. [[CrossRef](#)] [[PubMed](#)]
27. Dai, J.F.; Xian, T.; Di, L.J.; Yang, H. Preparation of BiFeO<sub>3</sub>-Graphene Nanocomposites and Their Enhanced Photocatalytic Activities. *J. Nanomater.* **2013**, *2013*, 642897. [[CrossRef](#)]
28. Yin, W.; Wang, W.; Sun, S. Photocatalytic degradation of phenol over cage-like Bi<sub>2</sub>MoO<sub>6</sub> hollow spheres under visible-light irradiation. *Catal. Commun.* **2010**, *11*, 647–650. [[CrossRef](#)]
29. Miyauchi, M. Photocatalysis and photoinduced hydrophilicity of WO<sub>3</sub> thin films with underlying Pt nanoparticles. *PCCP* **2008**, *10*, 6258–6265. [[CrossRef](#)] [[PubMed](#)]
30. Katsumata, H.; Taniguchi, M.; Kaneco, S.; Suzuki, T. Photocatalytic degradation of bisphenol A by Ag<sub>3</sub>PO<sub>4</sub> under visible light. *Catal. Commun.* **2013**, *34*, 30–34. [[CrossRef](#)]

31. Mousavi, M.; Habibi-Yangjeh, A.; Abitorabi, M. Fabrication of novel magnetically separable nanocomposites using graphitic carbon nitride, silver phosphate and silver chloride and their applications in photocatalytic removal of different pollutants using visible-light irradiation. *J. Colloid Interface Sci.* **2016**, *480*, 218–231. [[CrossRef](#)] [[PubMed](#)]
32. Liu, Y.; Fang, L.; Lu, H.; Liu, L.; Wang, H.; Hu, C. Highly efficient and stable Ag/Ag<sub>3</sub>PO<sub>4</sub> plasmonic photocatalyst in visible light. *Catal. Commun.* **2012**, *17*, 200–204. [[CrossRef](#)]
33. Shin, H.J.; Kim, K.K.; Benayad, A.; Yoon, S.M.; Park, H.K.; Jung, I.S.; Jin, M.H.; Jeong, H.K.; Kim, J.M.; Choi, J.Y.; et al. Efficient Reduction of Graphite Oxide by Sodium Borohydride and Its Effect on Electrical Conductance. *Adv. Funct. Mater.* **2009**, *19*, 1987–1992. [[CrossRef](#)]



© 2018 by the authors. Licensee MDPI, Basel, Switzerland. This article is an open access article distributed under the terms and conditions of the Creative Commons Attribution (CC BY) license (<http://creativecommons.org/licenses/by/4.0/>).